Talanta 281 (2025) 126804

Contents lists available at ScienceDirect

Talanta

journal homepage: www.elsevier.com/locate/talanta

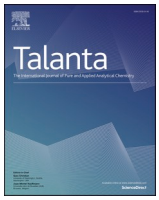

Separation of triacylglycerol (TAG) isomers by cyclic ion mobility mass spectrometry

Carlo R. de Bruin, Wouter J.C. de Bruijn, Mirjam A. Hemelaar, Jean-Paul Vincken, Marie Hennebelle *

Laboratory of Food Chemistry, Department of Agrotechnology and Food Sciences, Wageningen University, Wageningen, the Netherlands

ARTICLE INFO

Handling editor: María Dolores Luque de Castro

Keywords:
Isomeric lipids
cIMS-MS analysis
Adduct formation
Triglycerides
Space charge effects

ABSTRACT

Triacylglycerols (TAGs), a major lipid class in foods and the human body, consist of three fatty acids esterified to a glycerol backbone. They can occur in various isomeric forms, including sn-positional, *cis/trans* configurational, acyl chain length, double bond positional, and mixed type isomers. Separating isomeric mixtures is of great interest as different isomers can have distinct influence on mechanisms, such as digestibility, oxidative stability, or lipid metabolism. However, TAG isomer separation remains challenging with established analytical methodologies such as liquid-chromatography coupled to mass spectrometry (LC-MS). In this study, we developed a method with cyclic ion mobility mass spectrometry (cIMS-MS) for the separation and identification of all types of TAG isomers. First, the influence of different adducts (Li^+, NH_4^+, Na^+, and K^+) on the separation was studied. Overall, it was concluded that the sodium adduct is the best choice to efficiently separate all types of TAG isomers. In addition, trends were found in the influence of specific structural features on the drift time order. An order of relative influence (from high to low) was established; (1) degree of unsaturation of the fatty acid(s) on an exterior position (if the total degree of unsaturation(s) is equal in both TAGs), (2) acyl chain length on the exterior positions, (3) *cis/trans* configuration, and (4) double bond (DB)-position. Finally, various cIMS-MS strategies were developed for the separation of mixtures containing four, five, and six isomers. To conclude, the developed methods can be used for separation of complex mixtures of TAG isomers and have great potential to be expanded to isomers of similar types of lipids such as di- and monoacylglycerols. This study also shows the potential of cIMS-MS to be used for the application on real TAG samples.

1. Introduction

Triacylglycerols (TAGs) are a group of lipids that consist of three fatty acids esterified to a glycerol backbone. These compounds are the main constituents of food products such as oil(s) [1], but also have a major role in the human body via the metabolic pathways of energy storage and release [2]. Variations in their chemical structures affect TAGs physical (e.g., melting point and density) and physiological (e.g., digestibility and health benefits) properties, which consequently influence their functionalities. For instance, the distribution and content of saturated and unsaturated fatty acids in TAGs impacts the melting point, polymorphism, oxidative stability, digestibility, and health benefits of oils [1,3,4]. Besides this, smaller structural differences such as isomerism are also of importance and can influence TAGs functionalities in food (e.g., oxidative stability) and within the human body (e.g., digestibility) [3,5–10]. TAGs are versatile structures that can include five different types of isomers: sn-positional, *cis/trans* configuration, acyl chain length, double-bond position (DB-position), and mixed type isomers (Fig. 1). The mixed type occurs when multiple types are present simultaneously. To obtain a better understanding of the influence of TAG isomers on food characteristics or metabolic pathways in the human body, identification and characterization of these isomers is needed.

The characterization of TAGs is mostly done by gas chromatography coupled to flame ionization detection (GC-FID) or mass spectrometry (GC-MS) after derivatization, liquid chromatography coupled to evaporative light scattering detector (LC-ELSD) or mass spectrometry (LC-MS), and nuclear magnetic resonance (NMR) spectroscopy [11–16]. GC-FID and GC-MS are effective for the determination of fatty acid composition or TAG profiles when using an alternative technique as high

* Corresponding author. Laboratory of Food Chemistry, Department of Agrotechnology and Food Sciences, Wageningen University, Bornse Weilanden 9, 6708, WG, Wageningen, the Netherlands.
E-mail address: marie.hennebelle@wur.nl (M. Hennebelle).

https://doi.org/10.1016/j.talanta.2024.126804
Received 31 May 2024; Received in revised form 27 August 2024; Accepted 2 September 2024
Available online 3 September 2024

temperature-(HT)GC-FID [16]. Hence, these techniques typically do not give any information about the fatty acid sn-positional distribution. LC-MS can be used to separate and identify some but not all isomers, depending on the LC column characteristics. For example, some DB-position, *cis/trans,* and acyl chain isomers can be separated by LC using C18 columns (e.g., with charged surface hybrid materials). Sn-positional isomers can only be separated with targeted retention mechanisms such as polymeric C18 or silver-ion chromatography, or chiral columns in the case of enantiomers [17]. However, even when using such approaches, isobaric species can still overlap. This makes LC-MS not suitable for untargeted analysis of all lipid isomers and leads to challenges in identification of the TAGs [17]. In addition, LC remains time consuming. At last, NMR spectroscopy can also distinguish some isomers, albeit with limited resolution, but only if relatively pure samples and standards are measured. Thus, these aforementioned analytical techniques are not sufficient for the separation and identification of TAG isomers in complex mixtures. Unfortunately, real samples are almost always complex mixtures in which various isomers coexist.

An alternative and complementary technique for TAG isomer characterization is ion mobility spectrometry coupled to mass spectrometry (IMS-MS) [18,19]. Within IMS, ions are separated based on their mobility, which is related to the ion size, shape, and charge state [19]. Because of this, IMS can be very useful when separating lipid isomers. The established IMS techniques, such as drift-tube IMS (DTIMS) and travelling wave IMS (TWIMS), possess limited resolving power, which limits the resolution in the separation of lipid isomers [20,21]. Other IMS techniques with a higher resolving power such as differential-mobility spectrometry (DMS) and trapped IMS (TIMS) already showed some promising improvements for sn-positional, *cis/trans* and DB-position isomers when measured in pairs [22–24]. However, the achieved separation for these isomer types was still lacking resolution or in some cases, no separation was achieved at all. Therefore, multiple isomers could remain undetected in real samples that might contain more complex mixture of isomers and a higher resolving power in IMS is needed.

Cyclic ion mobility mass spectrometry (cIMS-MS) is a new state-of-the-art technique with increased resolving power. All details and geometry of the instrument are reported in the study of Giles et al. [25]. In short, higher resolving powers can be achieved because the path length can theoretically be extended infinitely (until wrap around or ion diffusion) by increasing the number of cycles of ions in the cyclic ion mobility racetrack. Separation using more than one pass is referred to as a multi-pass strategy. In addition, pre- and post-array storages can be used to store selected ions of interest. The pre-array storage can also induce fragmentation when accelerating the ions upon re-injection. With the use of pre- and post-array storages for repeated ion collection, reinjection, and ejection, IMS^n experiments can be performed on specific ions (precursor or fragments) to design advanced approaches for the separation of complex isomer mixtures [26]. The cIMS-MS has shown great potential for various kinds of complex isomer mixtures (e.g., flavonoids, oligosaccharides, and ribonucleotides) [27–29]. However, to the best of our knowledge, there have not yet been any reports on the improved separation of lipid isomers in general or TAG isomers specifically.

Besides using different instrumentation with a higher resolving power to achieve more separation (resolution), adduct formation can also be used as a tool in IMS [30]. When using ESI, cation adducts are usually formed following the addition of commercially available salts (e.g., ammonium acetate, commonly used in lipid analysis) to the analyte solution. This creates an interaction between the cations (e.g., NH_4^+, Na^+ or Li^+) and the analytes, forcing the formation of monomers (e.g., $[M + X]^+$) or multimers (e.g., $[2\ M + X]^+$) [31]. The formation of adducts changes the spatial conformation of the compounds. This can shift the mobility for one of the isomers due to the different coordination of the cation, and therefore, enhance the resolution [32]. However, no systematic evaluation has been done on which adduct provides the best IMS resolution for a specific class of lipid compounds. Therefore, the full potential of separating lipid, especially TAG, isomers with IMS has not yet been achieved.

The aim of this study was, therefore, to develop a versatile direct infusion cIMS-MS method for the separation of all types of TAG isomers. First, the influence of four common adducts, i.e., lithium, ammonium, sodium, and potassium, on the IMS resolution for all types of TAG isomers was evaluated. Then, the influence of structural properties (e.g., *cis* or *trans* configuration) on the drift time order was investigated to discover structure-mobility trends, which could be useful for the identification of unknown isomers in the future. At last, the capabilities of cIMS-MS to separate more complex mixtures were tested on multi-isomer samples containing four, five, and six isomers.

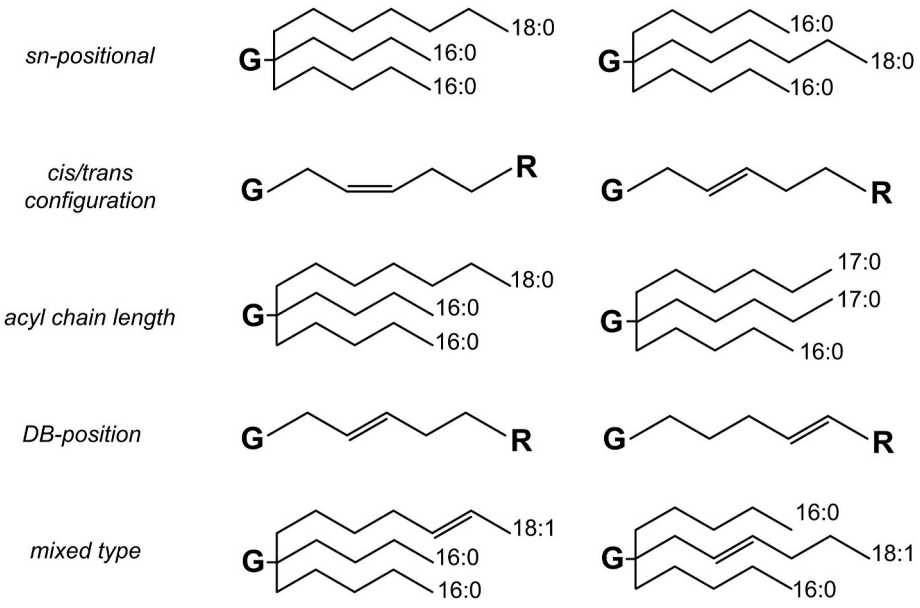

Fig. 1. Schematic representation of structural differences of the possible TAG isomer types: sn-position, *cis/trans* configuration, acyl chain length, double bond position (DB-position), and mixed type. (G = glycerol backbone; R = remainder of the acyl chain).

2. Materials & method

2.1. Chemicals

The TAG standards are listed in Table 1 and were purchased from Larodan B.V. (Solna, Sweden). All standards possessed a purity of at least >98 %. ULC/MS grade solvents including acetonitrile, isopropanol, methanol, and water were purchased from Biosolve (Valkenswaard, The Netherlands). Sodium iodide (>99 %) and lithium chloride (>99 %) powders were obtained from Sigma-Aldrich (St. Louis, MO, USA). Ammonium formate (>99 %) and potassium iodide (>99 %) powders were obtained from Biosolve (Valkenswaard, The Netherlands) and Honeywell (Seelze, Germany), respectively.

2.2. Sample preparation

The standards were dissolved in 99.9 % (*v/v*) isopropanol/water and prepared at concentrations between 400 and 600 ng mL^{-1}. Solutions of NaI, LiCl, NH_4HCO_2, and KI were individually added at final concentrations of 2 ng mL^{-1}, 0.4 ng mL^{-1}, 0.3 ng mL^{-1}, and 2.4 ng mL^{-1}, respectively. These concentrations were not optimized, but were found to be effective to induce constant formation of the corresponding adduct.

2.3. cIMS-MS analysis

The analysis was performed on a Select Series Cyclic Ion Mobility Mass Spectrometer (Waters Corporation, Wilmslow, U.K.). The instrument is described in detail by Giles et al. [25]. The cIMS instrument was configured for direct infusion analysis at a flow rate of 10 µL min^{-1} for most experiments. The system was flushed with 25 % *v/v/v/v* acetonitrile/isopropanol/methanol/water between samples. The MS acquisition was carried out with precursor selection in targeted MS^2 mode followed by IMS separation. Typical IMS parameters were travelling wave (TW) velocity of 700 m/s and TW static height of 50 V. For ionization, capillary and cone voltages of 2.5 kV and 40 V, respectively, were applied. The source temperature was set at 120 °C and the nitrogen desolvation gas flow at 800 L/h with a desolvation temperature of 300 °C. For trap fragmentation, a collision energy of 60–65 V was applied and for transfer fragmentation, 55–60 V. Nitrogen was used as collision and IMS gas. Within IMS^n experiments, top-and-tail and slicing strategies were used. A top-and-tail strategy consist of the ejection of unwanted ions out of the racetrack and subsequent additional separation of the remaining ions. A slicing strategy involves the ejection of unwanted ions out of the racetrack, ejection of specific ions of interest to the pre-array store, ejection of the remaining ions of interest out of the racetrack, reinjection of the ions within the pre-array store and separation of the reinjected ions in the racetrack (IMS^2). This sequence can be repeated multiple times (IMS^n) for specific ions of interests. All cIMS-MS separation strategies used in this work are visualized in Fig. 2. During all measurements, the intensity per MS scan was kept between 1.0×10^3 and 4.0×10^4 using the DRE lens to minimize space charge effects. A space charge effect is created by electrostatic repulsion (Coulombic interactions) between ions, which can cause peak broadening and create a shift in drift time [33]. Acquisition and processing were performed using MassLynx (version 4.2), UNIFI (version 1.8), Matlab (version R2019b), Microsoft Excel (version 2302), and R (version 4.0.2.).

2.4. Adduct evaluation study set-up

The adduct evaluation was performed using the prepared standards (Section 2.2) for all adducts: lithium, ammonium, sodium, and potassium. The samples were made by combining all the specific isomer pairs from the 25 standards, which resulted in 44 isomer pairs. These pairs are described and visualized in Tables S1 and S2. For each individual compound per adduct, the cycle time per pass was calculated (Table S3). This was done to measure and fairly compare all isomer pairs at the same resolving power for each adduct. Three numbers of passes were selected (i.e., 25, 50, and 100 passes in the cyclic tube) to allow the separation of most of the isomer pairs. After the measurements, the resolution (*Rs*) was calculated in Matlab for each isomer pair per adduct per number of passes (e.g., POP/PPO, Na^+, 25 passes) according to Eq. (1), in which Dt corresponds to the drift time and σ to the peak width at half height.

Table 1
List of all the TAG standards including systematic name, abbreviation, and the ratio of number of carbons and number of double bonds (C:N) in the fatty acid chains.

Systematic name	Abbreviation[a]	C:N	Molecular formula	Monoisotopic mass (Da)
1,2-Palmitin-3-stearin	PPS	50:0	$C_{53}H_{102}O_6$	834.77
1,2-Stearin-3-myristin	SSM	50:0	$C_{53}H_{102}O_6$	834.77
1,3-Palmitin-2-stearin	PSP	50:0	$C_{53}H_{102}O_6$	834.77
1,3-Stearin-2-myristin	SMS	50:0	$C_{53}H_{102}O_6$	834.77
1,2-Palmitin-3-elaidin	PPE	50:1	$C_{53}H_{100}O_6$	832.75
1,2-Palmitin-3-olein	PPO	50:1	$C_{53}H_{100}O_6$	832.75
1,3-Palmitin-2-elaidin	PEP	50:1	$C_{53}H_{100}O_6$	832.75
1,3-Palmitin-2-olein	POP	50:1	$C_{53}H_{100}O_6$	832.75
1,2-Stearin-3-olein	SSO	54:1	$C_{57}H_{108}O_6$	888.81
1,3-Stearin-2-olein	SOS	54:1	$C_{57}H_{108}O_6$	888.81
1-Arachidin-2-olein-3-palmitin	AOP	54:1	$C_{57}H_{108}O_6$	888.81
1-Arachidin-2-palmitin-3-olein	APO	54:1	$C_{57}H_{108}O_6$	888.81
1-Palmitin-2-arachidin-3-olein	PAO	54:1	$C_{57}H_{108}O_6$	888.81
1,3-Stearin-2-α-linolenin	SLnS	54:3	$C_{57}H_{104}O_6$	884.78
Tri-11(cis)*-octadecenoin*	VVV	54:3	$C_{57}H_{104}O_6$	884.78
Tri-6(trans)*-octadecenoin*	PlaPlaPla	54:3	$C_{57}H_{104}O_6$	884.78
Tri-6(cis)*-octadecenoin*	PliPliPli	54:3	$C_{57}H_{104}O_6$	884.78
Tri-9(trans)*-octadecenoin*	EEE	54:3	$C_{57}H_{104}O_6$	884.78
Triolein	OOO	54:3	$C_{57}H_{104}O_6$	884.78
1,2-Olein-3-linolein	OOL	54:4	$C_{57}H_{102}O_6$	882.77
1,3-Olein-2-linolein	OLO	54:4	$C_{57}H_{102}O_6$	882.77
1,2-Linolein-3-γ-linolenin	LLLnγ	54:7	$C_{57}H_{96}O_6$	876.72
1,2-Linolein-3-α-linolenin	LLLn	54:7	$C_{57}H_{96}O_6$	876.72
1,3-Linolein-2-γ-linolenin	LLnγL	54:7	$C_{57}H_{96}O_6$	876.72
1,3-Linolein-2- α-linolenin	LLnL	54:7	$C_{57}H_{96}O_6$	876.72

[a] A: Arachidic acid (20:0), E: Elaidic acid (18:1Δ9*t*), L: Linoleic acid (18:2Δ9*c*), Ln: α-Linolenic acid (18:3Δ9*c*), Lnγ: γ-Linolenic acid (18:3Δ6*c*), M: Myristic acid (14:0), O: Oleic acid (18:1Δ9*c*), P: Palmitic acid (16:0), Pla: Petroselaidic acid (18:1Δ6*t*), Pli: Petroselinic acid (18:1Δ6*c*), S: Stearic acid (18:0), V: Vaccenic acid (18:1Δ11*c*). The double bond number is counted from the glycerol backbone and *c* = *cis*, *t* = *trans*.

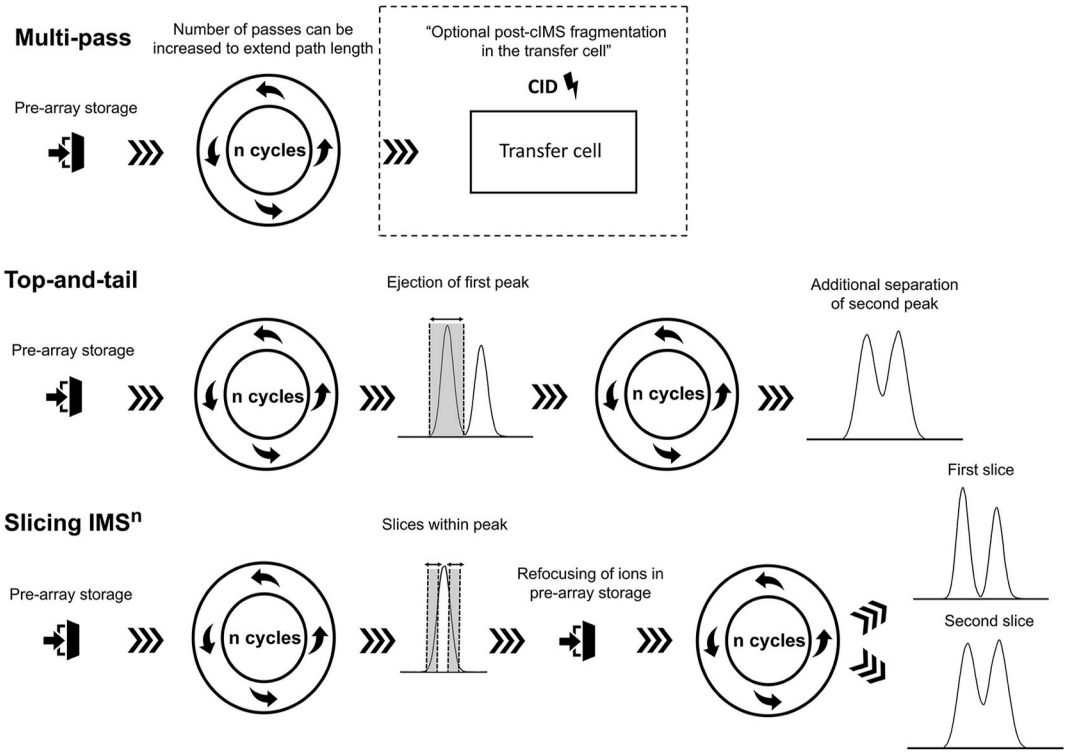

Fig. 2. Visualization of cIMS-MS separation strategies used in this work: multi-pass, top-and-tail, and slicing IMS^n.

$$\boldsymbol{Rs} = 1.18 * \frac{\mathrm{Dt2} - \mathrm{Dt1}}{\sigma 1 + \sigma 2} \quad \text{(Eq. 1)}$$

All isomers were measured as pairs and individuals, the data of the individuals was used to determine the drift time order of the isomers and the σ values. For each specific pair of isomers, the resolution at 50 and 100 passes was calculated only when no visible separation ($Rs < 0.4$) was observed at 25 and 50 passes, respectively. An example of visible separation is shown in the Supporting information (Fig. S1). During the data analysis, the efficiency of the different adducts to separate TAG isomers was eventually compared per isomer type (i.e., sn-positional, DB-position, *cis/trans* configuration, acyl chain length and mixed type) based on the following criteria: summed *Rs* values (i) and ratio between the number of separated pairs and total pairs tested (ii). Finally, the total (all isomer types combined) from each adduct was also compared per criterion. An example of the strategy is visualized in Fig. 3.

2.5. Confirmation of drift time order by statistical analysis

To illustrate the consistent nature of differences in drift time between an isomer pair, drift times of PSP and PPS were measured individually on three different timepoints within a day and on three different days using 25, 50, 75, and 100 passes. Next, using a one-way ANOVA in R studio (version 1.3.959), drift times were modelled using a factor for each isomer (PSP and PPS) and a block factor for the day effect. This approach effectively filters out the unwanted variation due to the day effect allowing for careful examination of the drift time differences unaffected by day effects. To facilitate comparisons in drift time order between the isomers, 95 % confidence intervals (CIs) were calculated to establish the drift time order per isomer. The CI values and average drift time per number of passes were used to derive a relative CI (%), which was used as a requirement to confirm the drift order of all isomer pairs within the study.

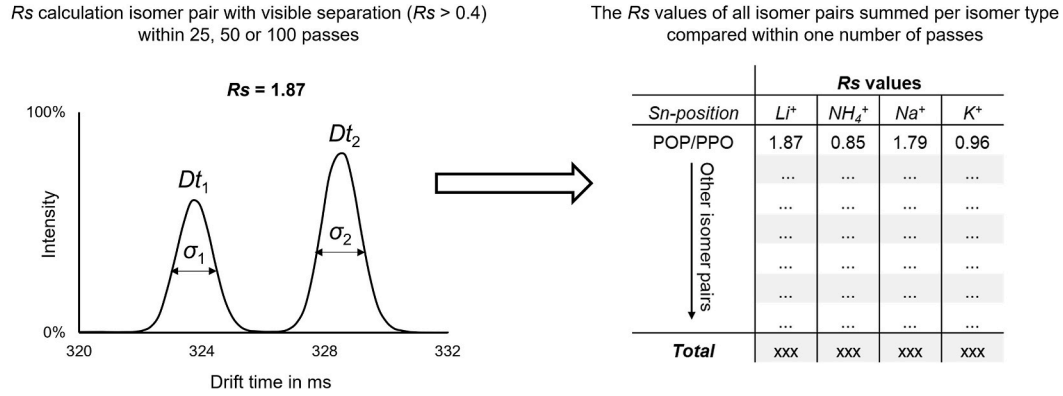

Fig. 3. Visualization of the strategy used to study the influence of adducts on isomer separation. Four adducts (Li^+, NH_4^+, Na^+, and K^+) were compared for 44 isomer pairs and at three numbers of passes (25, 50, and 100). In this example, the mobilogram of POP/PPO using the lithium adducts at 25 passes was used. The resolution was calculated for each set using Eq. (1) and all *Rs* values were summed within one number of passes for each isomer type.

3. Results & discussion

3.1. Adduct influence on isomer separation

To investigate the influence of adducts on TAG isomer separation, the performance of four different adducts (lithium, ammonium, sodium, and potassium) was compared for the separation of 44 isomer pairs (Table S1). Three multi-pass strategies of 25, 50, and 100 passes were used to evaluate the separation on all isomer pairs. An example of such a comparison is visualized in Fig. 4.

The adducts were compared per isomer type based on the summed *Rs* values, and the ratio between the number of separated pairs and total pairs (Table 2). The results of the 25, 50, and 100 passes were combined to obtain an overview of the total *Rs* per isomer type per adduct. Besides using the summed *Rs* values to evaluate the performances of the adducts, it was also checked whether the sum correlated with the number of highest *Rs* values within each isomer type (Tables S4–S6). This was checked to not over- or underestimate the performance of an adduct (e.g., the sodium adduct scores six highest values and two values of zero, which results in a higher sum of *Rs* values for the lithium adduct), and confirmed that it was indeed not the case for all comparisons. The *Rs* values per adduct per isomer pair per number of passes can be found in the Supporting information (Tables S4–S6).

In Table 2, the summed *Rs* values describe how well certain isomer types can be separated, while the ratio of separated pairs and total pairs describes the applicability across all isomer types. The summed *Rs* values of sodium presented the best results for all isomer types combined (total *Rs* of 37.9) and separately, except for DB-position isomers where ammonium performed the best. This can be useful information for specific applications regarding the separation of DB-position isomers. It is also noteworthy that ammonium and potassium performed in a similar way as they had small differences in *Rs* values for specific isomer types (Tables S4–S6), which was also seen for sodium and lithium. These differences in the performance of the adducts are probably related to the interaction sites between the molecules and the adduct ions. Adducts form due to electrostatic interactions such as ion-dipole interactions, where a different interaction site can lead to a different conformation of the resulting precursor ion and thus a different drift time [34,35]. In previous studies, correlations were found between the ionic radius and the resulting drift time for rigid structures, such as cannabinoids [32]. However, such correlations were not observed in the present study. No clear trend of increasing drift time with increasing ionic radius of the adduct ($Li^+ < Na^+ < K^+ < NH_4^+$) [36,37] was observed, and multiple differences were seen between compounds (isomer pairs excluded) (Table S3). The lack of relationship between ionic radius and drift time might be related to TAG molecules being less rigid and more flexible, thus being able to change their conformation depending on the adduct. To verify this, computational chemistry could be used to study potential interaction sites between the TAG molecules and the adduct ions, and conformations of the precursor ions [38]. This will be further discussed in Section 3.2.

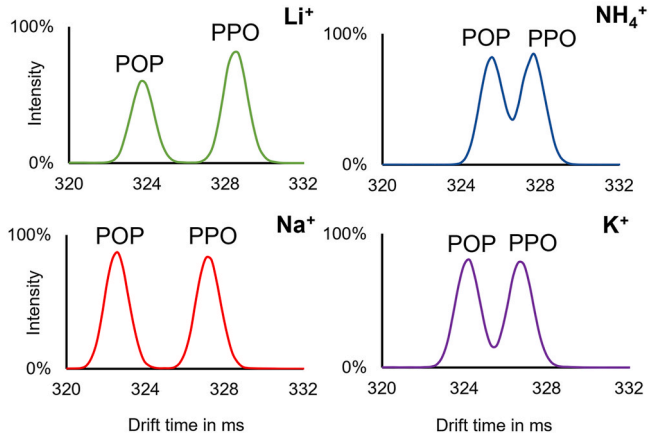

Fig. 4. Separation of the isomer pair POP/PPO using four adducts (Li^+, NH_4^+, Na^+, and K^+) at 25 passes.

For the ratio of separated pairs and total pairs, it can be seen that potassium performed the best with a ratio of 37/44 and therefore, seems the most widely applicable for TAG isomer separation. However, no big differences were observed between the different adducts, especially when taking into account the full range of 44 pairs. In addition, other parameters can still be assessed for the general applicability (e.g., ionization, fragmentation, and ion stability) in IMS-MS. For example, during our research, it was noted that potassium does not produce stable fragments when applying CID fragmentation compared to the other adducts. This would be a clear disadvantage for identification purposes when using this method for real samples such as oils. It is also important to note that the ratio is based on the pairs that show visible separation ($Rs > 0.4$) at 25, 50, or 100 passes. The pairs that do not show any visible separation could still be separated after more than 100 passes or by using individual standards to achieve minimal separation. Examples of such pairs are SLnS/PliPliPli, LLnL/LLLn, LLLn/LLnγL, LLnγL/LLnL, and PAO/APO. Their complex separation is shown in the Supporting information (Figs. S2, S3, S4, and S5). In Section 3.3, we will further discuss the separation of complex combinations of more than two isomers, including one set containing AOP, PAO, APO, SSO, and SOS (set B).

Overall, it can be concluded that the sodium adduct is the best choice to efficiently separate all types of TAG isomers. Therefore, the sodium adduct was used for further research on the structure influence on *Rs* and drift time (Section 3.2), and for the separation of multiple isomers simultaneously (Section 3.3). Yet, we acknowledge the fact that other adducts can still be used and tested for their separation.

3.2. Structure influence on resolution and drift time

Inter- and intra-day variations can cause drift times to shift, making absolute drift time unsuitable as an identifier. While drift time can typically be used to determine the collisional cross section (CCS) value - a physicochemical parameter related to the ion size and shape often used as an identifier - calibration is necessary when using a TWIMS-based technique [39]. Multi-pass strategies make CCS calibration more complex and despite recent improvements in CCS calibration for multi-pass

Table 2
Performance of different adducts (Li^+, NH_4^+, Na^+, and K^+)) for the effective separation of TAG isomers. The performance was compared based on the summed *Rs* values, and the ratio between the number of separated pairs and total pairs.

	Summed Rs *values*				Separated isomer pairs/Total isomer pairs			
Isomer type	Li^+	NH_4^+	Na^+	K^+	Li^+	NH_4^+	Na^+	K^+
Sn-position	8.4	5.1	9.8	6.3	8/11	10/11	9/11	10/11
Cis/Trans	3.6	3.1	4.0	3.2	4/4	4/4	4/4	4/4
Acyl chain	7.9	7.2	9.5	6.9	10/15	10/15	10/15	10/15
DB-position	1.7	5.2	3.9	4.8	4/6	6/6	5/6	6/6
Mixed type	10.5	7.9	10.7	9.2	7/8	6/8	7/8	7/8
Total	**32.1**	**28.5**	**37.9**	**30.4**	**33/44**	**36/44**	**35/44**	**37/44**

strategies [40], it is not yet possible to obtain sufficiently accurate CCS values to confidently distinguish closely related isomers, such as LLnL/LLLn/LLnγL/LLLnγ (Figs. S3 and S4). Thus, the drift time order of isomers is vital for their identification in complex samples. Requirements for using the drift time order in identification are that multiple isomers have to be present within the same measurement and that the order of the isomers should not change despite inter- and intra-day variations in drift time. To check whether this requirement was met in our analyses, the isomer standards PSP and PPS were individually measured with 25, 50, 75, and 100 passes on three different time points within a day and on three different days to determine whether the drift time order was reproducible by establishing a 95 % confidence interval (CI).

The statistical analysis resulted in a relative CI (%) of 0.07 % for all numbers of passes. All CI values of PSP and PPS per number of passes can be found in the Supporting information (Tables S7 and S8). Based on our results, it can be stated that the ΔDt between two isomers is sufficient when greater than 0.07 % of the average drift time of the two isomers. The difference in drift time of all isomer pairs in this study (Table 3) was larger than 0.07 % of the average drift time of the isomers. Thereby, we confirm that all the established drift time orders are reproducible.

In Table 3, the drift time orders of all isomer pairs are shown with the corresponding ΔDt. For most isomer pairs, the drift time order was determined from the number of passes that was used during the adduct influence study (Section 3.1). Alternatively, it was determined either with more passes and/or from specific separation strategies, which are discussed in more detail in Section 3.3. The observed drift time orders were the same for all adducts, except for the pair of PliPliPli/SLnS for which the sodium adduct had a different order than the other adducts. Besides the drift time orders, some interesting trends on the influence of specific structural features on the drift time order were noticed. These were categorized in trend numbers I-IV and shown per isomer combination. The trend numbers I-IV were explained in the footnote of Table 3.

Within the sn-positional isomers, two trends were observed in the drift time order. Firstly, when the fatty acid on an exterior position possesses more unsaturation in the chain, the drift time was higher (e.g., OLO < OOL) (trend I) Secondly, when the longer fatty acid (acyl chain length) in the TAG composition was present on an exterior position (sn-1/3), the drift time was also higher (e.g., PSP < PPS) (trend II). In some isomer pairs, actually both trends I and II were true (e.g., POP < PPO and PEP < PPE), making it hard to clearly distinguish which trend had the most influence on the specific drift time order. This question was clarified by looking at the drift time order of the isomers AOP/PAO/APO. PAO has the two shortest fatty acids in this composition (P and O) on the exterior positions, but it was slower (i.e., higher drift time) than AOP. The same trend was observed for the isomer pair SOS/PAO. Therefore, it can be concluded that an unsaturated fatty acid on an exterior position (O in this case) (trend I) has more influence on the drift time than the acyl chain length (trend II).

For the *cis/trans* isomers, TAGs having a fatty acid with the *cis* configuration systematically had a lower drift time compared to the *trans* configuration (trend III). From the *Rs* values in Section 3.1, it can be seen that TAGs with one difference of *cis/trans* (POP/PEP and PPO/PPE) were more difficult to separate than those with three differences (OOO/EEE and PliPliPli/PlaPlaPla). In addition, POP and PEP were more difficult to separate compared to PPO and PPE, which means that the *cis/trans* configuration has a larger influence on the drift time when present on an exterior position.

When looking at the position of the double bond in monounsaturated fatty acids, a DB-position further away from the glycerol backbone resulted in a lower drift time (trend IV). For example, when comparing VVV (11-*cis*), OOO (9-*cis*), and PliPliPli (6-*cis*), VVV had the lowest drift time, followed by OOO and PliPliPli. A similar trend was also observed with polyunsaturated fatty acids. For example, LLnL and LLLn (Ln: 9,12,15-*cis*) had a lower drift time compared to LLnγL and LLLnγ (Lnγ:

Table 3
The determined drift time order of each isomer pair at a certain number of passes with the corresponding difference in drift time (ΔDt), the average drift time (Dt) of the two separated peaks, and the main trend(s) that determine the drift time order. The systematic names and corresponding abbreviations of the TAGs can be found in Table 1.

Drift time order (shorter < longer)	Number of passes	ΔDt (ms)	Average Dt	*Trend (s)*[a]
Sn-positional				
PSP < PPS	100	3.43	1269.74	II
SSM < SMS	25	1.32	326.95	II
POP < PPO	25	4.75	324.98	I
PEP < PPE	25	5.54	326.16	I
SOS < SSO	25	2.91	351.51	I
OLO < OOL	25	1.85	336.19	I
LLnL < LLLn	235	4.49	3015.77	I
LLnγL < LLLnγ	50	2.11	656.50	I
PAO < APO	213	4.8	2820.00	II
AOP < APO	25	3.17	350.32	I
AOP < PAO	25	2.90	349.92	I
Cis/Trans				
POP < PEP	100	2.64	1235.22	III
PPO < PPE	100	5.28	1226.44	III
OOO < EEE	25	4.49	343.39	III
PliPliPli < PlaPlaPla	25	2.91	345.24	III
DB-position				
OOO < PliPliPli	25	2.90	341.74	IV
EEE < PlaPlaPla	50	2.64	664.47	IV
VVV < OOO	25	2.38	338.57	IV
VVV < PliPliPli	25	5.28	340.02	IV
LLnL < LLnγL	274	3.03	3513.14	IV
LLLn < LLLnγ	100	3.43	1299.04	IV
Acyl chain				
SSM < PPS	50	2.37	639.46	II
PSP < SMS	50	2.37	640.45	II
SSM < PSP	100	1.40	1220.10	NA[e]
PPS < SMS	100	1.10	1224.65	II
APO < SSO[b]	42	1.32	571.81	NA[e]
SOS < APO	25	2.64	351.11	I
OOO < SLnS	25	3.43	334.75	NA[d]
SLnS < EEE	100	3.69	1295.94	NA[d]
PliPliPli < SLnS[c]	195	4.88	2520.33	NA[d]
SLnS < PlaPlaPla	25	2.38	337.78	NA[d]
VVV < SLnS	25	6.08	339.89	NA[d]
SOS < PAO	25	2.11	350.32	I
PAO < SSO[b]	42	1.32	571.81	II
AOP < SOS[b]	42	0.66	566.99	NA[e]
AOP < SSO	25	3.43	350.19	I
Mixed types				
OOO < PlaPlaPla	25	5.81	343.46	III, IV
PliPliPli < EEE	25	1.32	344.04	III
POP < PPE	25	5.54	324.51	I, III
PEP < PPO	25	3.96	318.24	I
VVV < EEE	25	6.86	340.68	III, IV
VVV < PlaPlaPla	25	4.75	334.68	III, IV
LLnL < LLLnγ	50	2.37	655.63	I
LLnγL < LLLn	274	3.83	3515.98	I, IV

[a] I: Higher degree of unsaturation(s) of the fatty acid on an exterior position (sn-1/3) is slower than on the interior position (sn-2) if the total degree of unsaturation is equal in both TAGs. II: A longer acyl chain on an exterior position (sn-1/3) is slower than a longer chain on the interior position (sn-2). III: *trans* configurations are slower than *cis* configurations. IV: A lower double bond position (closer to the glycerol backbone) is slower than a higher double bond position.

[b] For these pairs the difference in drift time of the deconvoluted peaks was used (see Section 3.3, Fig. 6).

[c] The presented drift time order for this specific isomer pair was as determined for the sodium adduct. The drift time order for the lithium, ammonium, and potassium adducts was reversed.

[d] NA, not applicable. Too many mixed isomer types/structural differences to define a clear trend.

[e] No clear trend could be determined for this acyl chain length isomer, because the total acyl chain length on the exterior positions was equal with one longer and one shorter chain.

6,9,12-*cis*), respectively. However, the *Rs* values (Tables S4–6) showed that the pairs LLnL/LLnγL and LLLn/LLLnγ were more difficult to separate than VVV, OOO, and PliPliPli, which was probably caused by the presence of multiple DB-positions in Ln and Lnγ.

Within the set of acyl chain isomer pairs (Tables S1 and S2), the pairs without an identical fatty acid on the same sn-position such as SOS/PAO and PSP/SMS were relatively easily separated, whereas the pairs with an identical fatty acid on the same sn-position, such as SSM/PSP or AOP/SOS, were difficult to separate. It was also observed that when the identical fatty acid was present on an exterior position, more separation was observed than if it was present on the interior position. This again confirmed the trend of the larger influence of the fatty acids on the exterior positions on the drift time. Some of these isomer pairs could only be distinguished by deconvolution using specific fragments or by measuring the individual standards, which is further discussed in Section 3.3. After establishing trends I-IV from the isomer types, i.e., sn-positional, *cis/trans*, DB-position, and acyl chain, the mixed type isomers were used to investigate whether one trend had more influence on the drift time than another.

The mixed type isomers consist of isomer pairs with multiple isomer types and, therefore, more than one trend coexists. From these pairs, the trends were compared for their relative influence on the drift time. For example, from the pair PliPliPli (6-*cis*) and EEE (9-*trans*), it was concluded that the *cis/trans* configuration (trend III) had more influence on the drift time compared to DB-position (trend IV), because PliPliPli had a lower drift time than EEE. This is further exemplified by the pair of PEP/PPO, for which PEP had the lower drift time. Thus, the influence of the acyl chain length on the exterior positions (trend II) in PEP or the unsaturation on an exterior position in PPO (trend I) was greater than the influence of *cis* (PPO) and *trans* (PEP) configuration (trend III). Indeed, from the aforementioned results, it was determined that the *cis* configuration should result in a lower drift time, which is not the case in this pair. The same trend was observed for the pair POP/PPE. At last, the pair of LLnγL and LLLn indicated that the degree of unsaturation on an exterior position (trend I) had more influence than the difference in DB-position (trend IV) (Lnγ; 6-*cis*, 9-*cis*, 12-*cis* compared to Ln; 9-*cis*, 12-*cis*, 15-*cis*), as LLnγL has a lower drift time than LLLn.

Based on all the observed trends from the mixed types and the isomer cases AOP/PAO/APO and SOS/PAO, the following order of the relative influence of the different structural features on the drift time was established, from high to low: (1) degree of unsaturation of the fatty acid (s) on an exterior position (if the total degree of unsaturation(s) is equal in both TAGs), (2) acyl chain length on the exterior positions, (3) *cis/trans* configuration, and (4) DB-position. These trends can provide valuable information for the potential identification of unknown isomers in the future. For follow-up research, a dedicated computational study with a modelling technique, such as density functional theory (DFT), could be useful to explain these trends in more detail. Molecular dynamics for instance, could give more insights into the adduct interaction sites. Besides a computational study, development of methods for accurate CCS calibrations for multi-pass strategies in cIMS are necessary to simplify and strengthen the identification of TAG isomers.

3.3. cIMS-MS capabilities for multiple isomers

In real TAG samples (e.g., oil) containing complex mixtures of TAGs, it is expected that multiple isomers can be present. In such cases, LC separation is typically applied prior to MS detection and identification of the TAGs. It is likely that not all isomers can be separated by LC, thus multiple isomers will enter the MS at the same time. This prevents confident identification of the individual TAGs by MS, which could be tackled by cIMS-MS. However, despite being able to separate pairs of TAG isomers with cIMS-MS using our method, a different cIMS-MS strategy might be required for separation of multiple (>2) isomers. To mimic this challenge, three sets of multiple isomer mixtures including all types were prepared: Set A consisted of four isomers including POP, PPO, PEP, and PPE; set B consisted of five isomers including APO, SOS, PAO, AOP, and SSO; and set C consisted of six isomers including OOO, EEE, PliPliPli, PlaPlaPla, VVV, and SLnS. Each set was infused and a specific IMS or IMS^n strategy was performed to elucidate their multiple

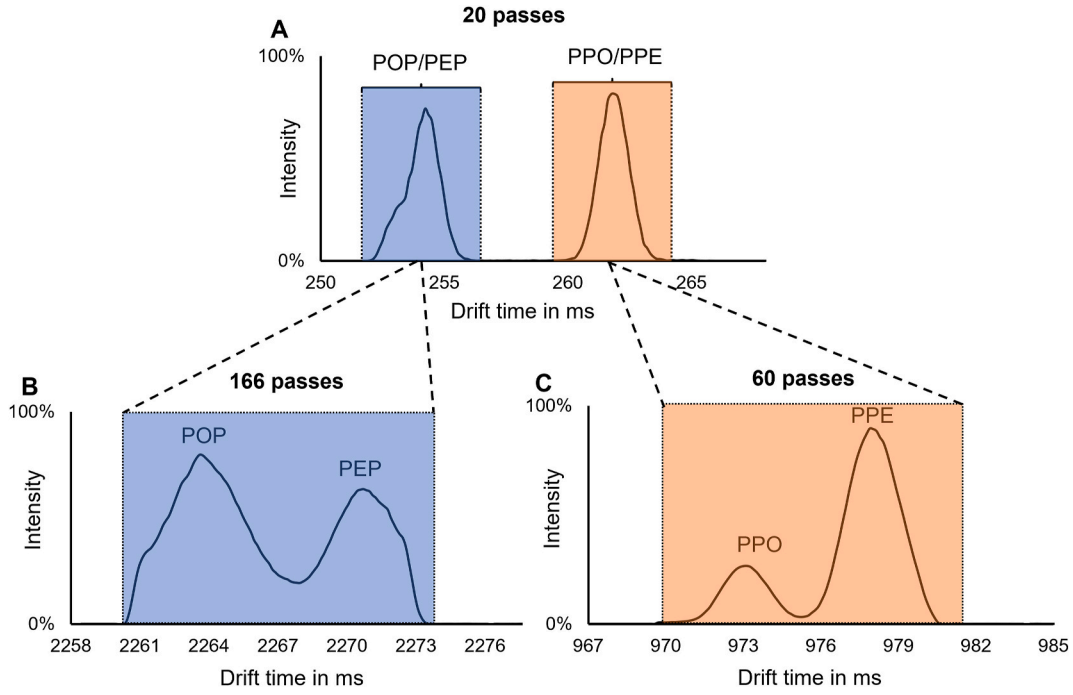

Fig. 5. Separation of the isomers within set A (POP/PPO/PEP/PPE) using a top-and-tail strategy. The precursor mass of 855.73 was selected in MS^2 and an initial separation of 20 passes was used within cIMS to separate POP/PEP (1st peak) and PPO/PPE (2nd peak) (A). Top-and-tail was applied both on the first (B) and second peak (C) by ejection-retainment-separation steps. The first peak (B) was separated with 166 additional passes and the second peak (C) was separated with 60 additional passes.

isomers simultaneously. These specific strategies are necessary as without them the peak capacity of the cIMS dimension is not enough to achieve visible separation of all isomers simultaneously. Using these strategies, limitations of cIMS separation due to wrap around and extensive peak broadening are circumvented. Figs. 5–7 show the results of set A-C, respectively.

All isomers in set A were successfully separated with the top-and-tail strategy presented in Fig. 5. The initial separation between POP/PEP and PPO/PPE with a high *Rs* was achieved relatively easily after 20 passes. Top-and-tail strategies (Fig. 5B & C) were applied by ejecting one of the two pairs of isomers, while retaining the other one for separation. After ejection of the ions from PPO/PPE, the isomers POP/PEP were separated after a total of 186 passes, i.e., with an additional 166 passes (Fig. 5B). Adding more passes did not have any additional value as the separation cannot be further improved due to peak broadening. After ejection of the ions from POP/PEP, the isomers PPO/PPE were well separated after a total of 80 passes (Fig. 5C), which is clearly less than the amount of passes used for POP and PEP. The difference in separation (i.e., needed amount of passes) between the pairs POP/PEP and PPO/PPE is related to the *cis/trans* configurations on different sn-positions as discussed in Section 3.2. In addition, the drift time order of POP < PEP < PPO < PPE correlated well with the observed results in Section 3.2. The applied top-and-tail strategy was necessary to obtain well separated peaks of all the isomers because an extended multi-pass strategy would have led to wrap around effects and loss of separation. The advantage of the top-and-tail strategy is that the initial separation (Fig. 5A) is not lost and the second separation step (Fig. 5B and C) can be used as additional passes. The disadvantage of a top-and-tail strategy is that ions can diffuse and the amount of ions (signal) will become less. This is not the case for an alternative slicing IMS^n strategy were ions are ejected to the pre-array store, which refocuses the ions upon reinjection. On the other hand, the initial separation will get lost when using a slicing strategy.

The separation of the isomers within set B was done with a post-cIMS fragmentation strategy. The separation was more complex as the mixture contains TAGs that have a nearly identical drift time (Section 3.1 and 3.2), especially acyl chain isomers with one identical fatty acid on the same sn-position did not show any visible separation. Acyl chain length isomers have a different fatty acid composition, which creates the possibility to distinguish them based on their specific fragments. When fragmenting a sodiated TAG, the neutral loss of each fatty acid results in multiple sodiated and protonated DAG fragments (Fig. 6B) [41,42]. A strategy was created involving a multi-pass separation of 42 passes followed by CID fragmentation in the transfer cell. The 42 passes resulted in two well separated peaks (Fig. 6A), where the first peak consists of AOP/SOS and the second peak of PAO/APO/SSO. In the first peak, no separation can be seen between AOP and SOS. When observing the fragments in the spectrum (Fig. 6B), specific (DAG) fragments were found, which can be used to deconvolute the TAG isomers in the mobilogram (Fig. 6A). The neutral loss of stearic acid (M−S) is specific for SOS and SSO and therefore the separation can be seen between AOP/SOS and PAO/SSO and APO/SSO. For PAO/APO, no visible separation was achieved in this complex mixture. However, their visible separation was shown with an extension of passes (Fig. S5). On the other hand, different adducts were more effective for the specific separation of PAO/APO, as ammonium and potassium showed visible separation (*Rs* 1.0 for both) after 100 passes (Tables S4–S6). Therefore, it could be favorable to form multiple adducts (e.g., sodium and potassium) simultaneously to extract the maximum out of the potential separation for all isomers. In the case where no visible separation can be achieved, isomers can still be distinguished by measuring the individual standards or by deconvolution using specific fragment ratios [43,44]. In the end, the post-cIMS fragmentation strategy used for set B was quick and successful despite the lack of separation between PAO/APO in Fig. 6. In addition, the same strategy was also performed successfully on a comparable set of isomers including SSM/PSP/PPS/SMS. These results are shown in the Supporting information (Fig. S6). As a perspective on real

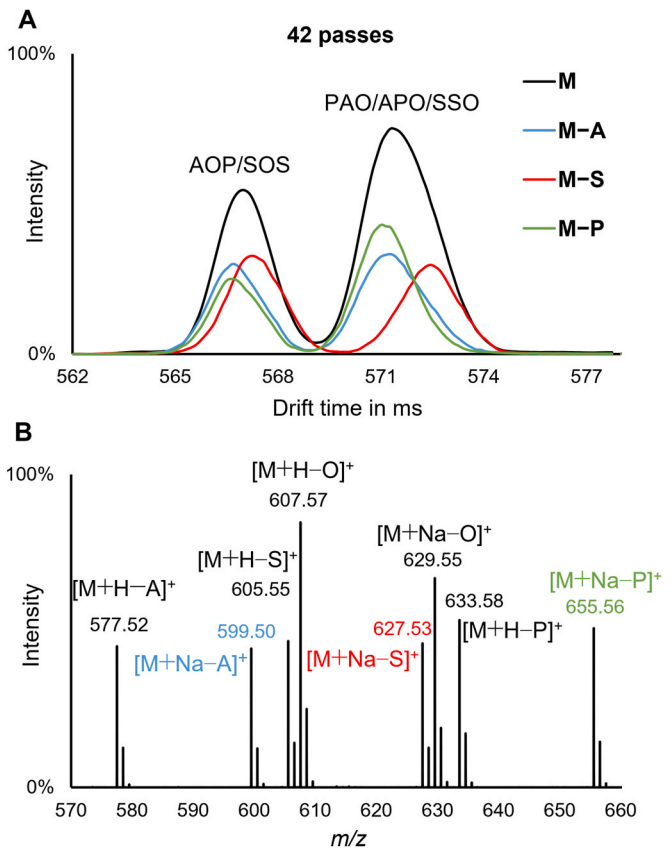

Fig. 6. Separation of the isomers within set B (AOP/SOS/PAO/APO/SSO) using a post-cIMS fragmentation strategy. A multi-pass separation was followed by fragmentation (55 V) in the transfer cell. The initial separation of 42 passes was used to separate AOP/SOS (1st peak) and PAO/APO/SSO (2nd peak) (A). Fragmentation of the precursor *m/z* 911.79 (M) delivered a spectrum with the characteristic diacylglycerol (DAG) fragments as sodiated and protonated ions (B). The specific sodiated fragment ions (M−A, M−S, M−P) were visualized in the mobilogram to achieve deconvolution for separation of the isomers.

sample applications (e.g., oils with unknown composition), this strategy would be a suitable first step for isomer screening, as fragmentation spectra with specific fragments or fragment ratios are likely needed for identification of the isomers. Additionally, the trends established in this work can be used as final confirmation or for tentative identification when the difference between the fragmentation spectra is too small.

In Fig. 7, the six isomers of set C were also separated by a top-and-tail strategy, but with an additional slicing (IMS^2) step. From the results in Section 3.1, it was known that some isomers (e.g., OOO/PlaPlaPla) would show high resolution separation while others not (SLnS/PliPliPli), which made the eventual strategy complex and extensive. Firstly, an initial separation of 25 passes was used to separate the isomers as much as possible, followed by the ejection of the VVV and OOO ions (A1). Secondly, the retained isomers (PliPliPli/SLnS/EEE/PlaPlaPla) were separated by 55 additional passes, followed by the ejection of the PlaPlaPla ions (B1). Afterwards, PliPliPli/SLnS and EEE were separated by 63 additional passes, which was followed by the slicing step (C1). The ions of PliPliPli/SLnS were ejected to the pre-array store and refocused, while the ions of EEE were ejected from the racetrack. Because of the refocusing of the ions within the pre-array store, the previously achieved separation was lost. At the end, 158 new passes needed to be applied in the last step to separate PliPliPli and SLnS (D1). This last slicing step was necessary, because it was complex to move the peak of EEE to the front of the mobilogram without losing too many ions of PliPliPli/SLnS. This was due to the low resolution separation between PliPliPli/SLnS and EEE, which makes the accurate ejection of ions difficult. The refocusing

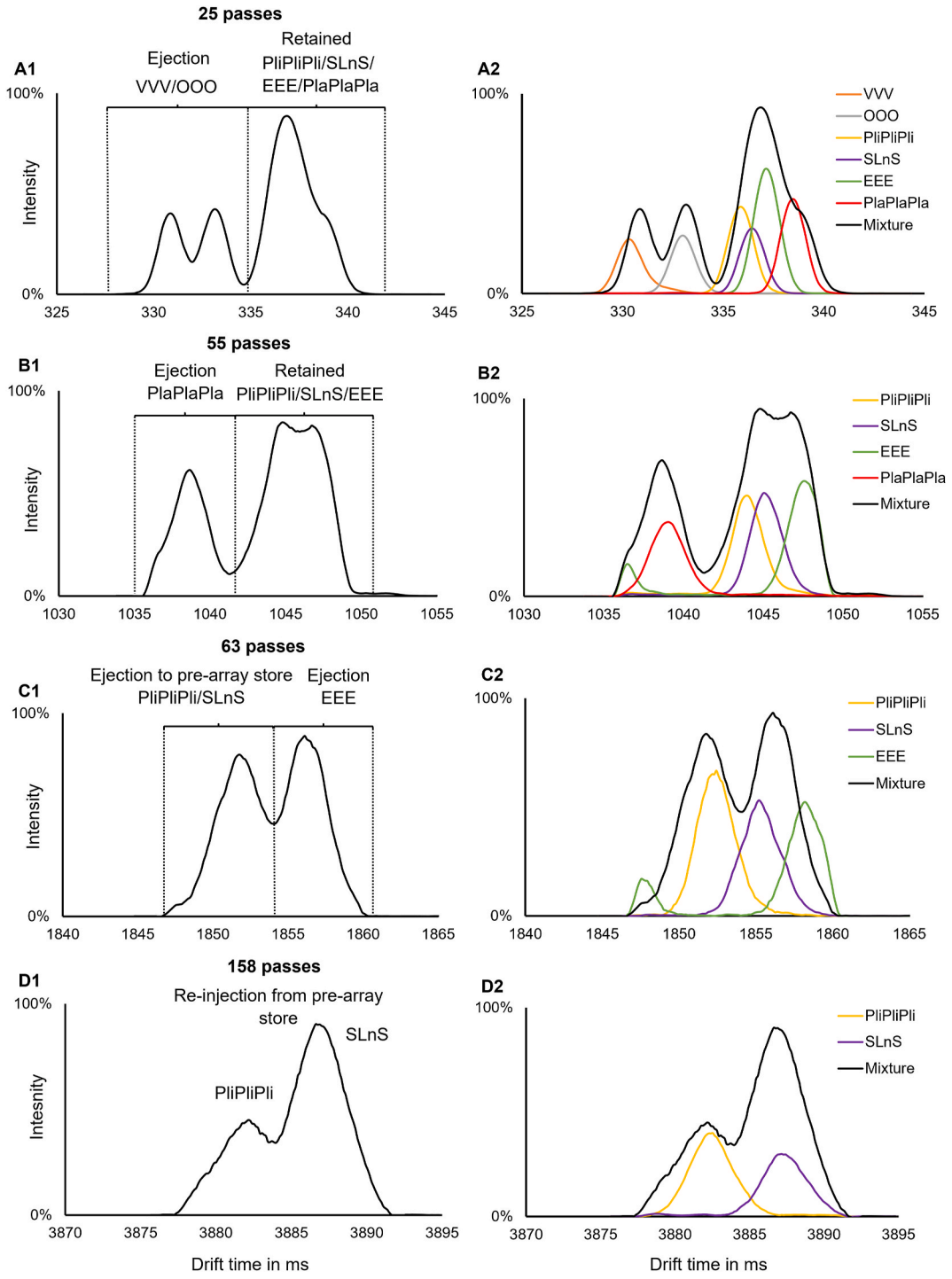

Fig. 7. Separation of the isomers within set C (VVV/OOO/PliPliPli/SLnS/EEE/PlaPlaPla) using a top-and-tail and slicing IMS^2 strategy. The precursor mass of 907.76 was selected in MS^2 and an initial separation of 25 passes was used to separate VVV and OOO from PliPliPli/SLnS/EEE/PlaPlaPla and the ions of VVV and OOO were ejected out of the racetrack (A1). The second step (B1) involved the separation of PlaPlaPla from PliPliPli/SLnS/EEE with 55 additional passes followed by the ejection of PlaPlaPla. The third step (C1) involved the separation of PliPliPli/SLnS and EEE with 63 additional passes, whereafter the ions of PliPliPli/SLnS were ejected to the pre-array store and EEE was ejected. At the last step, all the previous passes were lost and PliPliPli/EEE were separated after 158 passes. The mobilograms of the individual compounds (coloured lines) are overlayed with the mobilograms of the mixtures (Fig. 7 A2-D2).

of the ions created a disadvantage as the number of passes doubled. On the other hand, the refocusing of ions can also be used as an advantage when dealing with ion diffusion and peak broadening along a high number of passes (i.e., long pathlength).

Fig. 7 (A2-D2) shows the measured individual isomers with the same strategy. Identification using individuals standards within such strategies can be tricky as it was difficult to control the amount of ions per isomer in the racetrack. Space charge effects in particular will increase when using more passes and higher amounts of ions. These effects can lead to peak shifting and subsequently to false identifications. This is demonstrated in the Supporting information (Fig. S7), in which it can be seen that there was a small shift in drift time when comparing 100 passes measured at an intensity per MS scan of 1.0×10^3 and 5.0×10^4. The intensity per MS scan gives a relative indication of the amount of ions in

the racetrack. To demonstrate the issues that can occur due to space charge effects, another experiment was performed on set C where the individuals were measured at relatively low intensities of 3.0×10^4 to 4.0×10^4 per MS scan. The results of this experiment are shown in the Supporting information (Fig. S8), where space charge effects increased along many more passes, which eventually led to considerable shifts in drift times and could lead to false identifications. By keeping the intensity per MS scan as low as possible, the influence of space charge effects can be minimized. Therefore, the measured set C and individual standards (Fig. 7 A2-D2) were measured at a low intensity ($1.0–5.0*10^3$) per MS scan. Another challenge caused by space charge effects was peak broadening. In such extensive strategies, this cannot be prevented. Peak broadening causes challenges with ejecting unwanted ions accurately. As peaks overlap, ions that need to be retained will be partly ejected as well, which leads to a loss of signal.

Besides these challenges, our results demonstrate that cIMS-MS has a lot of potential for the complex separation of multiple TAG isomers including multiple isomer types. For future perspectives, the hyphenation of LC with cIMS-MS can simplify the use of such strategies as some isomer types could be separated with LC. For example, Fouque et al. have shown some separation of glycerophosphatidylcholine (PC) and DAG *cis/trans* and DB-position isomers within the LC dimension [23]. Because of this, we expect that our cIMS-MS method hyphenated with LC has great future potential for the characterization of TAG isomers within complex samples such as oil. However, some challenges still need to be addressed. One of these challenges is that real samples may contain high concentrations of certain TAGs, consequently excessively high amounts of ions entering the racetrack might result in peak shifting due to space charge effects. This does not influence the drift time order of isomers because all isomers will shift similarly, but can interfere with CCS determinations that may be used for identification in the future (see discussion in Section 3.2). To control space charge effects as much as possible, the most straightforward option would be to automate control of the DRE lens in the mass spectrometer, which regulates the amount of ions that enter the cyclic racetrack. Unfortunately, this is not possible yet with the current operating software. Another challenge is that there are a few isomers that are very difficult to separate (e.g., LLnL/LLnγL), which need several seconds to obtain separation. This could potentially give issues in hyphenation with LC, especially for chromatographic peaks that are only a few seconds wide. Nonetheless, the majority of TAG isomers can be separated in a few hundred milliseconds in cIMS.

4. Conclusion

In this study, a powerful cIMS-MS method was developed for TAG isomer separation. Overall, of the four tested adducts (lithium, ammonium, sodium, and potassium), sodium produced the best results and is therefore the suggested adduct to use for TAG isomer separation. An order in drift time between 44 tested isomer pairs was established, which led to observation of recurring structure-mobility trends between and within the isomer types. An order of influence from high to low was established: degree of unsaturation of the fatty acid(s) on an exterior position (if the total degree of unsaturation(s) is equal in both TAGs), acyl chain length on the exterior positions, *cis/trans* configuration, and DB-position. Furthermore, the separation of complex multi-isomer sets (4, 5, and 6 isomers) was successfully achieved by developing specific cIMS-MS strategies, including top-and-tail and slicing IMS^2. We believe that the method developed here can be used for separation and characterization of TAG isomers in complex mixtures and has great potential to be expanded to isomers of similar types of lipids, such as di- and monoacylglycerols.

Notes

The authors declare no competing financial interest.

CRediT authorship contribution statement

Carlo R. de Bruin: Writing – original draft, Visualization, Methodology, Investigation, Formal analysis, Data curation, Conceptualization. **Wouter J.C. de Bruijn:** Writing – review & editing, Supervision, Resources, Methodology, Conceptualization. **Mirjam A. Hemelaar:** Writing – review & editing, Methodology, Data curation. **Jean-Paul Vincken:** Writing – review & editing, Supervision, Resources. **Marie Hennebelle:** Writing – review & editing, Supervision, Resources, Methodology, Conceptualization.

Declaration of competing interest

The authors declare that they have no known competing financial interests or personal relationships that could have appeared to influence the work reported in this paper.

Data availability

Data will be made available on request.

Acknowledgements

The authors would like to acknowledge and thank Mark Sanders, Edwin Bakx, and Bram van de Put for their technical assistance. Additionally, we would like to acknowledge and thank Dr. Jos Hageman for his assistance with the statistical analysis. The presented results were obtained using a Waters Select Series Cyclic Ion Mobility Mass Spectrometer which is owned by WUR-Shared Research Facilities. Investment by WUR-Shared Research Facility was made possible by the 'Regio Deal Foodvalley'.

Appendix A. Supplementary data

Supplementary data to this article can be found online at https://doi.org/10.1016/j.talanta.2024.126804.

References

[1] F.J. Hidalgo, R. Zamora, Triacylglycerols: structures and properties, Encyclopedia of Food and Health (2016) 351–356, https://doi.org/10.1016/B978-0-12-384947-2.00702-9.
[2] M. Ahmadian, R.E. Duncan, K. Jaworski, E. Sarkadi-Nagy, H.S. Sul, Triacylglycerol metabolism in adipose tissue, Future Lipidol. 2 (2007) 229–237, https://doi.org/10.2217/2F17460875.2.2.229.
[3] J.E. Hunter, Studies on effects of dietary fatty acids as related to their position on triglycerides, Lipids 36 (7) (2001) 655–668, https://doi.org/10.1007/s11745-001-0770-0.
[4] D. Swanson, R. Block, S.A. Mousa, Omega-3 fatty acids EPA and DHA: health benefits throughout life, Adv. Nutr. 3 (1) (2012) 1–7, https://doi.org/10.3945/an.111.000893.
[5] K.M. Linderborg, H.P.T. Kallio, Triacylglycerol fatty acid positional distribution and postprandial lipid metabolism, Food Rev. Int. 21 (3) (2005) 331–355, https://doi.org/10.1080/FRI-200061623.
[6] T. Karupaiah, K. Sundram, Effects of stereospecific positioning of fatty acids in triacylglycerol structures in native and randomized fats: a review of their nutritional implications, Nutr. Metab. 4 (2007) 16, https://doi.org/10.1186/1743-7075-4-16.
[7] A. Alfieri, E. Imperlini, E. Nigro, D. Vitucci, S. Orrù, A. Daniele, et al., Effects of plant oil interesterified triacylglycerols on lipemia and human health, Int. J. Mol. Sci. 19 (1) (2018) 104, https://doi.org/10.3390/2Fijms19010104.
[8] F. Bar-Yoseph, Y. Lifshitz, T. Cohen, Review of sn-2 palmitate oil implications for infant health, Prostaglandins Leukotrienes Essential Fatty Acids 89 (4) (2013) 139–143, https://doi.org/10.1016/j.plefa.2013.03.002.
[9] J.C. Bakala-N'Goma, L. Couëdelo, C. Vaysse, M. Letisse, V. Pierre, A. Géloen, et al., The digestion of diacylglycerol isomers by gastric and pancreatic lipases and its impact on the metabolic pathways for TAG re-synthesis in enterocytes, Biochimie 203 (2022) 106–117, https://doi.org/10.1016/j.biochi.2022.01.003.
[10] C. Wijesundera, C. Ceccato, P. Watkins, P. Fagan, B. Fraser, N. Thienthong, et al., Docosahexaenoic acid is more stable to oxidation when located at the sn-2 position of triacylglycerol compared to sn-1(3), JAOCS (J. Am. Oil Chem. Soc.) 85 (2008) 543–548, https://doi.org/10.1007/s11746-008-1224-z.

[11] M. Li, E. Butka, X. Wang, Comprehensive quantification of triacylglycerols in soybean seeds by electrospray ionization mass spectrometry with multiple neutral loss scans, Sci. Rep. 4 (2014) 6581, https://doi.org/10.1038/2Fsrep06581.
[12] X.Y. Dong, J. Zhong, F. Wei, X. Lv, L. Wu, Y. Lei, et al., Triacylglycerol composition profiling and comparison of high-oleic and normal peanut oils, JAOCS (J. Am. Oil Chem. Soc.) 92 (2015) 233–242, https://doi.org/10.1007/s11746-014-2580-5.
[13] N. Kobayashi, E.A. Noel, A. Barnes, J. Rosenberg, C. Dirusso, P. Black, et al., Rapid detection and quantification of triacylglycerol by HPLC-ELSD in *Chlamydomonas reinhardtii* and *Chlorella* strains, Lipids 48 (10) (2013) 1035–1049, https://doi.org/10.1007/s11745-013-3828-9.
[14] R. Garcia, A. Pires, N. Martins, T. Carvalho, A.J. Burke, M.J. Cabrita, Assessment of the triacylglycerol fraction of olive oil by 1D-NMR spectroscopy: exploring the usefulness of DEPT tool on the peak assignments of ^{13}C NMR spectra, European Food Research and Technology 245 (2019) 2479–2488, https://doi.org/10.1007/s00217-019-03359-0.
[15] L. Fauconnot, F. Robert, R. Villard, F. Dionisi, Chemical synthesis and NMR characterization of structured polyunsaturated triacylglycerols, Chem. Phys. Lipids 139 (2) (2006) 125–136, https://doi.org/10.1016/j.chemphyslip.2005.11.004.
[16] Y. Qian, M. Rudzińska, A. Grygier, R. Przybylski, Determination of triacylglycerols by HTGC-FID as a sensitive tool for the identification of rapeseed and olive oil adulteration, Molecules 25 (17) (2020) 3881, https://doi.org/10.3390/molecules25173881.
[17] M. Fabritius, B. Yang, Analysis of triacylglycerol and phospholipid sn-positional isomers by liquid chromatographic and mass spectrometric methodologies, Mass Spectrom. Rev. (2023) 1–33, https://doi.org/10.1002/mas.21853.
[18] G. Paglia, A.J. Smith, G. Astarita, Ion mobility mass spectrometry in the omics era: challenges and opportunities for metabolomics and lipidomics, Mass Spectrom. Rev. 41 (5) (2021) 722–765, https://doi.org/10.1002/mas.21686.
[19] M. Hernández-Mesa, D. Ropartz, A.M. García-Campaña, H. Rogniaux, G. Dervilly-Pinel, B. Le Bizec, Ion mobility spectrometry in food analysis: principles, current applications and future trends, Molecules 24 (2019) 15–2706, https://doi.org/10.3390/molecules24152706.
[20] J.E. Kyle, X. Zhang, K.K. Weitz, M.E. Monroe, Y.M. Ibrahim, R.J. Moore, et al., Uncovering biologically significant lipid isomers with liquid chromatography, ion mobility spectrometry and mass spectrometry, Analyst 141 (2016) 1649–1659, https://doi.org/10.1039/C5AN02062J.
[21] X. Zheng, R.D. Smith, E.S. Baker, Recent advances in lipid separations and structural elucidation using mass spectrometry combined with ion mobility spectrometry, ion-molecule reactions and fragmentation approaches, Curr. Opin. Chem. Biol. 42 (2018) 111–118, https://doi.org/10.1016/j.cbpa.2017.11.009.
[22] A.P. Bowman, R.R. Abzalimov, A.A. Shvartsburg, Broad separation of isomeric lipids by high-resolution differential ion mobility spectrometry with tandem mass spectrometry, J. Am. Soc. Mass Spectrom. 28 (8) (2017) 1552–1561, https://doi.org/10.1007/s13361-017-1675-2.
[23] K.J.D. Fouque, C.E. Ramirez, R.L. Lewis, J.P. Koelmel, T.J. Garrett, R.A. Yost, et al., Effective liquid chromatography-trapped ion mobility spectrometry-mass spectrometry separation of isomeric lipid species, Anal. Chem. 91 (8) (2019) 5021–5027, https://doi.org/10.1021/acs.analchem.8b04979.
[24] M. Šala, M. Lísa, J.L. Campbell, M. Holčapek, Determination of triacylglycerol regioisomers using differential mobility spectrometry, Rapid Commun. Mass Spectrom. 30 (2) (2016) 256–264, https://doi.org/10.1002/rcm.7430.
[25] K. Giles, J. Ujma, J. Wildgoose, S. Pringle, K. Richardson, D. Langridge, et al., A cyclic ion mobility-mass spectrometry system, Anal. Chem. 91 (13) (2019) 8564–8573, https://doi.org/10.1021/acs.analchem.9b01838.
[26] J. Ujma, D. Ropartz, K. Giles, K. Richardson, D. Langridge, J. Wildgoose, et al., Cyclic ion mobility mass spectrometry distinguishes anomers and open-ring forms of pentasaccharides, J. Am. Soc. Mass Spectrom. 30 (6) (2019) 1028–1037, https://doi.org/10.1007/s13361-019-02168-9.
[27] C.R. de Bruin, M. Hennebelle, J.-P. Vincken, W.J.C. de Bruijn, Separation of flavonoid isomers by cyclic ion mobility mass spectrometry, Anal. Chim. Acta 1244 (2023) 340774, https://doi.org/10.1016/j.aca.2022.340774.
[28] T. Kenderdine, R. Nemati, A. Baker, M. Palmer, J. Ujma, M. FitzGibbon, et al., High-resolution ion mobility spectrometry-mass spectrometry of isomeric/isobaric ribonucleotide variants, J. Mass Spectrom. 55 (2) (2020) e4465, https://doi.org/10.1002/jms.4465.
[29] Peterson TL, Nagy G. Toward sequencing the human milk glycome: high-resolution cyclic ion mobility separations of core human milk oligosaccharide building blocks. Anal. Chem., 93, 27, 9397–9407, .oi:10.1021/acs.analchem.1c00942.
[30] D. Hadavi, E. de Lange, J. Jordens, Y. Mengerink, F. Cuyckens, M. Honing, Adduct ion formation as a tool for the molecular structure assessment of ten isomers in traveling wave and trapped ion mobility spectrometry, Rapid Commun. Mass Spectrom. 33 (S2) (2019) 49–59, https://doi.org/10.1002/rcm.8419.
[31] S.M. Camunas-Alberca, M. Moran-Garrido, J. Sáiz, A. Gil-de-la-Fuente, C. Barbas, A. Gradillas, Integrating the potential of ion mobility spectrometry-mass spectrometry in the separation and structural characterisation of lipid isomers, Front. Mol. Biosci. 10 (2023) 1112521, https://doi.org/10.3389/fmolb.2023.1112521.
[32] B.M. Zietek, Y. Mengerink, J. Jordens, G.W. Somsen, J. Kool, M. Honing, Adduct-ion formation in trapped ion mobility spectrometry as a potential tool for studying molecular structures and conformations, International Journal for Ion Mobility Spectrometry 21 (2018) 19–32, https://doi.org/10.1007/s12127-017-0227-6.
[33] V. Ilbeigi, M. Tabrizchi, Peak-peak repulsion in ion mobility spectrometry, Anal. Chem. 84 (8) (2012) 3669–3675, https://doi.org/10.1021/ac3001447.
[34] Y. Huang, E.D. Dodds, Ion mobility studies of carbohydrates as group I adducts: isomer specific collisional cross section dependence on metal ion radius, Anal. Chem. 85 (20) (2013) 9728–9735, https://doi.org/10.1021/ac402133f.
[35] B.H. Clowers, H.H. Hill, Influence of cation adduction on the separation characteristics of flavonoid diglycoside isomers using dual gate-ion mobility-quadrupole ion trap mass spectrometry, J. Mass Spectrom. 41 (3) (2006) 339–351, https://doi.org/10.1002/jms.994.
[36] C. Peng, G. Wang, L. Qin, S. Luo, F. Min, X. Zhu, Molecular dynamics simulation of NH_4-montmorillonite interlayer hydration: structure, energetics, and dynamics, Appl. Clay Sci. 195 (2020) 105657, https://doi.org/10.1016/j.clay.2020.105657.
[37] Y. Marcus, Thermodynamics of solvation of ions. Part 5. - gibbs free energy of hydration at 298.15 K, J. Chem. Soc., Faraday Trans. 87 (1991) 2995–2999, https://doi.org/10.1039/FT9918702995.
[38] D. Hadavi, M. Borzova, T. Porta Siegel, M. Honing, Uncovering the behaviour of ions in the gas-phase to predict the ion mobility separation of isomeric steroid compounds, Anal. Chim. Acta 1200 (2022) 339617, https://doi.org/10.1016/j.aca.2022.339617.
[39] J.N. Dodds, E.S. Baker, Ion mobility spectrometry: fundamental concepts, instrumentation, applications, and the road ahead, J. Am. Soc. Mass Spectrom. 30 (11) (2019) 2185–2195, https://doi.org/10.1007/s13361-019-02288-2.
[40] S.C. Habibi, G. Nagy, General method to obtain collision cross-section values in multipass high-resolution cyclic ion mobility separations, Anal. Chem. 95 (20) (2023) 8028–8035, https://doi.org/10.1021/acs.analchem.3c00919.
[41] W. Gazlay, J.J. Evans, The impact of the complexing agent on the sensitivity of collision-induced dissociation spectra to fatty acid position for a set of XYZ-type triglycerides, Rapid Commun. Mass Spectrom. 36 (4) (2022) e9226, https://doi.org/10.1002/rcm.9226.
[42] P. Makarov, D. Zheng, D. Le, J.J. Evans, Impact of the complexing cation on the sensitivity of collision-induced dissociation spectra to fatty acid position for a set of YXY/YYX-type triglycerides, Rapid Commun. Mass Spectrom. 32 (18) (2018) 1591–1598, https://doi.org/10.1002/rcm.8211.
[43] B. Harper, E.K. Neumann, S.M. Stow, J.C. May, J.A. McLean, T. Solouki, Determination of ion mobility collision cross sections for unresolved isomeric mixtures using tandem mass spectrometry and chemometric deconvolution, Anal. Chim. Acta 939 (2016) 64–72, https://doi.org/10.1016/j.aca.2016.07.031.
[44] B. Zekavat, T. Solouki, Chemometric data analysis for deconvolution of overlapped ion mobility profiles, J. Am. Soc. Mass Spectrom. 23 (11) (2012) 1873–1884, https://doi.org/10.1007/s13361-012-0471-2.